Article

Glucose Conversion into 5-Hydroxymethylfurfural over Niobium Oxides Supported on Natural Rubber-Derived Carbon/Silica Nanocomposite

Rujeeluk Khumho [1,2], Satit Yousatit [1,2] and Chawalit Ngamcharussrivichai [1,2,3,*]

[1] Department of Chemical Technology, Faculty of Science, Chulalongkorn University, Pathumwan, Bangkok 10330, Thailand; faiirujeeluk@gmail.com (R.K.); y.satit@hotmail.com (S.Y.)
[2] Center of Excellence in Catalysis for Bioenergy and Renewable Chemicals (CBRC), Faculty of Science, Chulalongkorn University, Pathumwan, Bangkok 10330, Thailand
[3] Center of Excellence on Petrochemical and Materials Technology (PETROMAT), Chulalongkorn University, Pathumwan, Bangkok 10330, Thailand
* Correspondence: chawalit.ng@chula.ac.th; Tel.: +66-2218-7528; Fax: +66-2255-5831

Abstract: 5-Hydroxymethylfurfural (HMF) is one of the most important lignocellulosic biomass-derived platform molecules for production of renewable fuel additives, liquid hydrocarbon fuels, and value-added chemicals. The present work developed niobium oxides (Nb_2O_5) supported on mesoporous carbon/silica nanocomposite (MCS), as novel solid base catalyst for synthesis of HMF via one-pot glucose conversion in a biphasic solvent. The MCS material was prepared via carbonization using natural rubber dispersed in hexagonal mesoporous silica (HMS) as a precursor. The Nb_2O_5 supported on MCS (Nb/MCS) catalyst with an niobium (Nb) loading amount of 10 wt.% (10-Nb/MCS) was characterized by high dispersion, and so tiny crystallites of Nb_2O_5, on the MCS surface, good textural properties, and the presence of Bronsted and Lewis acid sites with weak-to-medium strength. By varying the Nb loading amount, the crystallite size of Nb_2O_5 and molar ratio of Bronsted/Lewis acidity could be tuned. When compared to the pure silica HMS-supported Nb catalyst, the Nb/MCS material showed a superior glucose conversion and HMF yield. The highest HMF yield of 57.5% was achieved at 93.2% glucose conversion when using 10-Nb/MCS as catalyst (5 wt.% loading with respect to the mass of glucose) at 190 °C for 1 h. Furthermore, 10-Nb/MCS had excellent catalytic stability, being reused in the reaction for five consecutive cycles during which both the glucose conversion and HMF yield were insignificantly changed. Its superior performance was ascribed to the suitable ratio of Brønsted/Lewis acid sites, and the hydrophobic properties generated from the carbon moieties dispersed in the MCS nanocomposite.

Keywords: 5-hydroxymethylfurfural; glucose; carbon/silica nanocomposite; niobium oxide; acidity

1. Introduction

Nowadays, the world has been confronted with environmental and economic crises, which are related to the dependence of human activities on petroleum-derived fuels and chemicals. Moreover, conventional petroleum reservoirs are likely to be depleted in the future [1–3]. Lignocellulosic biomass, mainly consisting of cellulose (40–50 wt.%), is an abundant renewable resource for sustainable production of energy, fuels, and chemicals based on the biorefinery concept. Hydrolysis of cellulose yields glucose, which can be then transformed into high-quality biofuels and a wide variety of high value-added chemicals through different catalytic processes [4,5]. 5-Hydroxymethylfurfural (HMF) is ranked as a top-twelve biomass-derived platform molecules by the United States Department of Energy [6]. Due to the presence of both hydroxyl and aldehyde functional groups in its molecule, HMF is a potential intermediate for production of renewable fuel additives, liquid hydrocarbon fuels, and specialty chemicals in polymer, food, and pharmaceutical industries [7].

Production of HMF from glucose is an acid-catalyzed two-consecutive reaction process, in which glucose is firstly isomerized into fructose and then dehydrated into HMF. Homogeneous Lewis and Brønsted acids are respectively used to catalyze the reactions, which renders the process environmentally unfriendly, and causes corrosion problems of reactor systems [8]. To overcome these problems, a number of studies have been devoted to the development of heterogeneous acid catalysts for converting glucose into HMF, such as cation exchange resins, metal oxides, metal phosphates, zeolites, and carbon-based materials [1,4,7].

Niobium (Nb)-based catalysts are a class of metal oxides, which exhibit a strong acidic character, high chemical and thermal stability, and good performance in the HMF synthesis [9]. The Nb^{5+} ions serve as Lewis acid centers responsible for the glucose–fructose isomerization, while the fructose dehydration is mainly catalyzed by Nb–OH species with Brønsted acidity [10]. In addition, niobium oxides (Nb_2O_5) have been identified as solid acids with excellent water-resistant properties [11,12]. Various materials, such as beta zeolite [6], mesoporous silica SBA-15 [13], and carbon [5], have been investigated as supports for Nb-based catalysts for glucose conversion into HMF in biphasic water- organic solvent systems. However, a low initial concentration of glucose feedstock (or a high catalyst loading level) and a substantial formation of humins limited the practical use of these catalysts. Recently, Lin et al. [14] synthesized alumina (γ-Al_2O_3) functionalized with alkyl groups a hydrophobic acid catalyst for HMF synthesis from fructose, while Yang et al. [15] designed a series of hydrophobic silica nanoparticles for catalytic conversion of glucose into HMF. The effect of hydrophobic properties on retardation of HMF condensation to form humins was addressed.

Mesoporous carbon/silica nanocomposites (MCS) have attracted considerable attention in the catalytic processes for conversion of biomass-derived carbohydrates into HMF and other renewable chemicals [16]. The mesostructured silica framework provides good textural properties and thermal stability, while the carbon moieties possess hydrophobic properties that could reduce the formation of humins [14]. In addition, the carbon surface is covered with oxygen-functional groups, such as hydroxyl (−OH) and carboxyl (−COOH), which improved the adsorption of substrate molecules and dispersion of active metal species on the catalyst surface [17,18]. Conventionally, the MCS materials are prepared by infiltration of carbon precursors, such as glucose, furfuryl alcohol, phenol, and formaldehyde, into preformed mesoporous silica, followed by carbonization or hydrothermal treatment [17,18]. Natural rubber (NR) is a renewable elastomer that can be extracted from the *Hevea brasiliensis* tree [19]. It is mainly composed of poly(*cis*-1,4-isoprene), and fully biodegradable. Thailand is one of the world's leading producers of NR. Due to its chemical composition and hydrophobic nature, it has been used as a renewable source for preparation of polymer/silica nanocomposites with high mesoporosity for adsorption and catalysis [20–23]. Recently, we successfully prepared the MCS materials with tunable textural and hydrophobic properties using hexagonal mesoporous silica (HMS) and NR as a mesostructured framework and carbon source, respectively [23], which found potential application as a drug carrier.

In this work, we prepared a series of Nb-based catalysts using pure silica HMS and NR-derived MCS nanocomposite as supports. The obtained catalysts were characterized for their physicochemical properties using various techniques and then were applied to the glucose conversion into HMF in a biphasic solvent of aqueous sodium chloride solution and tetrahydrofuran. Effects of the support type, Nb loading amount, catalyst loading level, reaction temperature and time on the glucose conversion and the product's yield were investigated. Moreover, the catalyst recyclability was evaluated to realize the practical use of our developed catalysts.

2. Results and Discussion

2.1. Physicochemical Properties of Nb/HMS and Nb/MCS Catalysts

The thermogravimetric (TG) and differential thermal analysis (DTA) curves of HMS and MCS are compared in the Supplementary Material (SM); Figure S1. Both pure silica HMS and MCS nanocomposite exhibited the weight loss between room temperature and 100 °C, which corresponded to physisorbed moisture (3–4 wt.%). The weight loss observed for MCS at 300–650 °C was ascribed to the decomposition of carbon in the silicate framework (13.3 wt.%). Moreover, MCS showed a small loss of weight (2.4 wt.%) in the range of 200–300 °C, which was related to the oxygen-functional groups on the carbon surface [24].

The X-ray photoelectron spectroscopy (XPS) was used to identify the type of surface functional groups of MCS as shown in Figure S2 (SM). The C1s XPS spectrum can be decomposed into four peaks, comprised of carbon groups (C=C, CH$_x$, and C–C), hydroxyl groups or ether linkages (C–O, C–O–C), carbonyl groups (C=O), and carboxyl or ester groups (O–C=O) at 283.6, 285.7, 287.3, and 289.0 eV, respectively [25,26]. These results confirmed the presence of the carbon moieties and oxygen functional groups, such as hydroxyl group (–OH) and carboxyl group (–COOH) [24], in the MCS nanocomposite.

The X-ray diffraction (XRD) patterns and nitrogen (N$_2$) physisorption isotherms of HMS, NR/HMS and MCS are shown in Figure 1. All samples exhibited the reflection peak at 2θ in the range of 20–25° (Figure 1A), which corresponded to amorphous silica [27,28]. When compared to HMS, NR/HMS showed an increased intensity of amorphous phase since the incorporated NR hindered the condensation of silicate framework of HMS. The carbonization used in the MCS preparation promoted the formation of siloxane bond (Si–O–Si), decreasing the amorphous nature of the silica matrix. The N$_2$ physisorption isotherms revealed the mesoporous character of these materials (Figure 1B), according to the IUPAC classification. Compared to the pristine HMS, the mesoporosity of NR/HMS and MCS was relatively lower (Table 1) due to the presence of organic moieties dispersed in the mesostructure framework [23].
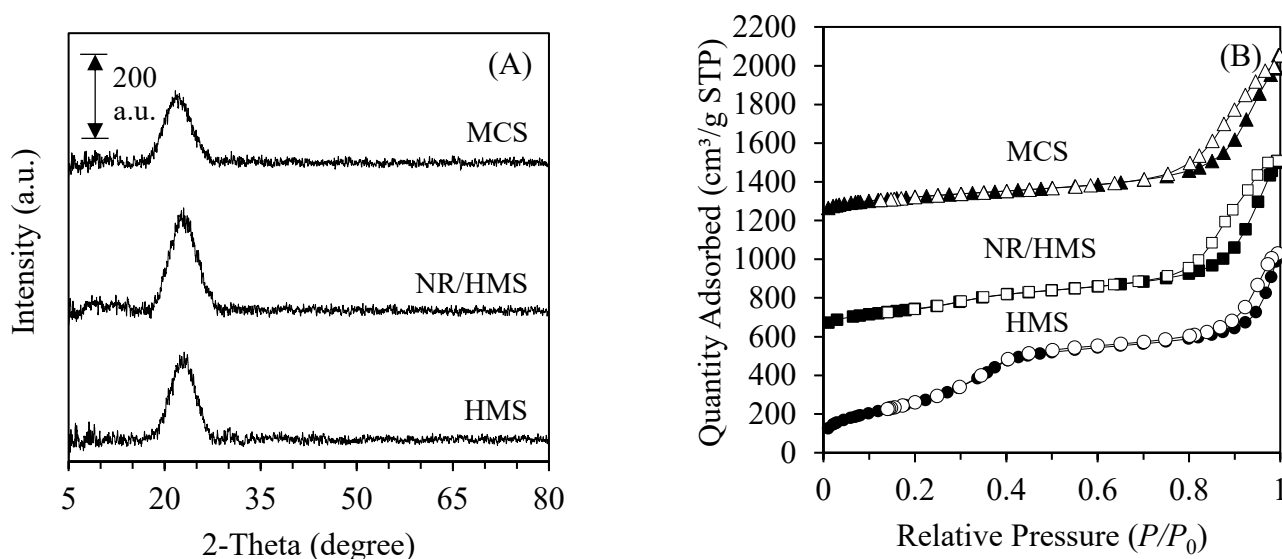

Figure 1. (**A**) XRD patterns and (**B**) N$_2$ physisorption isotherms of HMS, NR/HMS, and MCS.

The XRD patterns of the Nb/HMS and Nb/MCS with different Nb loading amounts are shown in Figure 2A,B, respectively. The characteristic peaks of Nb$_2$O$_5$ were not observed for both 10-Nb/HMS and 10-Nb/MCS, indicating the small crystallites of Nb$_2$O$_5$ well dispersed on the HMS and MCS surface. An increase in the amount of Nb loaded on the HMS and MCS surface to 20 and 30 wt.% enhanced the characteristic peaks of Nb$_2$O$_5$ at 2θ = 22.6°, 28.5°, 36.7°, 46.2°, 50.5°, 55.2°, 64.2° and 70.8° [29], which indicate the enlarged

Nb_2O_5 particles [30]. The crystallite size of Nb_2O_5 on HMS (39.7–47.4 nm) was smaller than that on MCS (45.8–49.0 nm). It was explained by a higher surface area for HMS than MCS (Table 1) [31]. As shown in Figure 2C, the images obtained from transmission microscopy (TEM) confirmed a high dispersion of Nb_2O_5 crystallites on both the HMS and MCS surface but formed agglomerates at an increased Nb loading level.
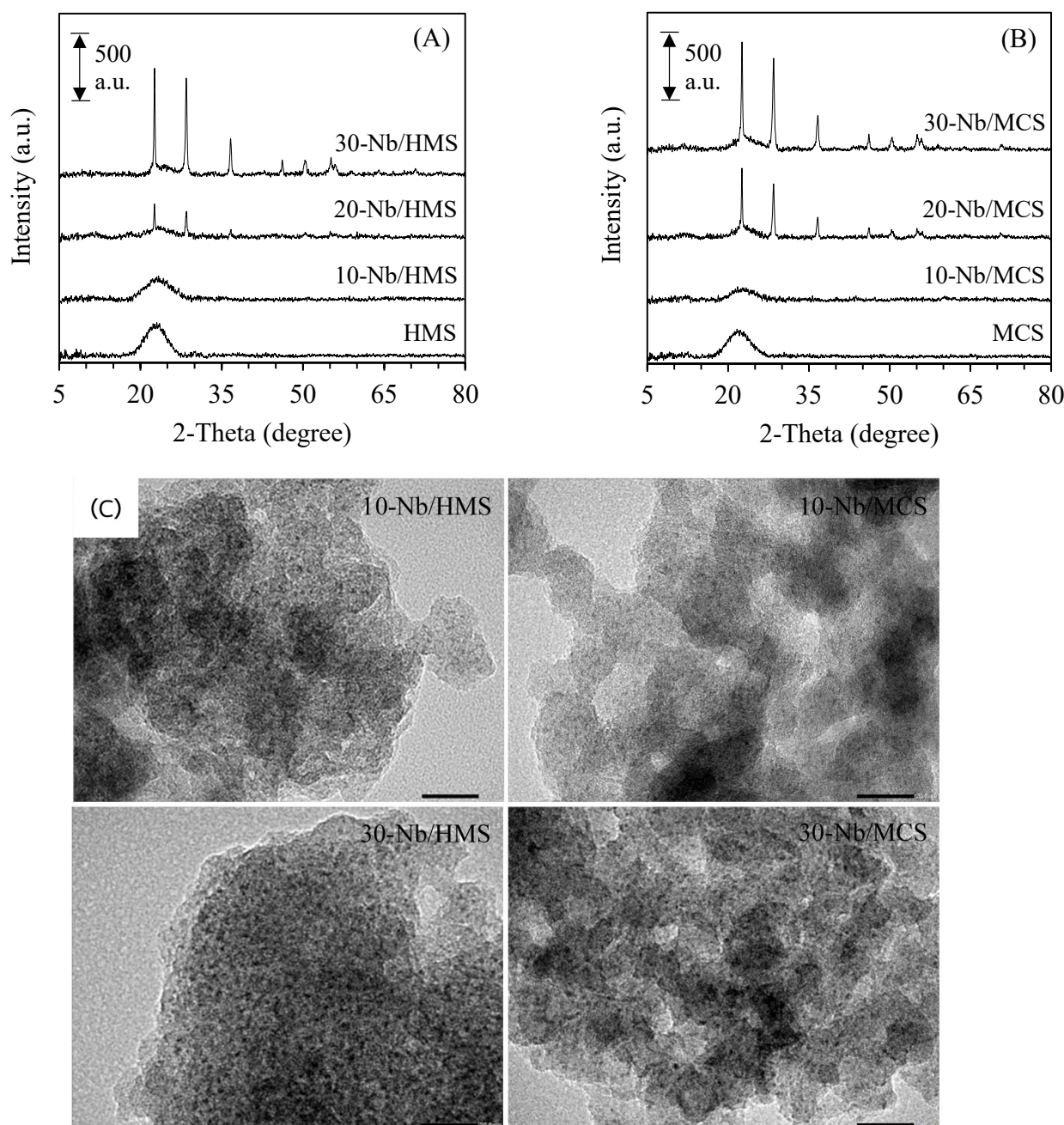

Figure 2. (**A**,**B**) XRD patterns of (**A**) *X*-Nb/HMS and (**B**) *X*-Nb/MCS catalysts, and (**C**) TEM images of representative *X*-Nb/HMS and *X*-Nb/MCS catalysts at magnification of 400,000×.

The N_2 adsorption-desorption isotherms indicated that the mesoporous nature of HMS and MCS was retained after the Nb loading (Figure 3). The textural parameters of these catalysts are summarized in Table 1. The impregnation of Nb onto both HMS and MCS decreased S_{BET}, V_t, and D_p, which confirmed the presence of Nb_2O_5 species dispersed on the surface of mesostructured HMS and MCS [32]. Furthermore, with increasing the amount of Nb loading, the Nb/HMS series exhibited a relatively large reduction of textural

properties when compared to the Nb/MCS samples. To rationalize the advantage of MCS in this aspect, the field-emission scanning electron microscopy (FE-SEM) was carried out (Figure 4). Both of the pristine HMS and MCS exhibited tiny spherical particles (Figure 4A,B, respectively), which were conformed to the previous work [24]. The Nb loading resulted in a significant agglomeration of 10-Nb/HMS particles (Figure 4C), while the morphology of 10-Nb/MCS remained unchanged (Figure 4D). These results implied that the carbon moieties in the MCS nanocomposite created a hydrophobic environment, which could reduce the interaction, and so the agglomeration, between silica particles.
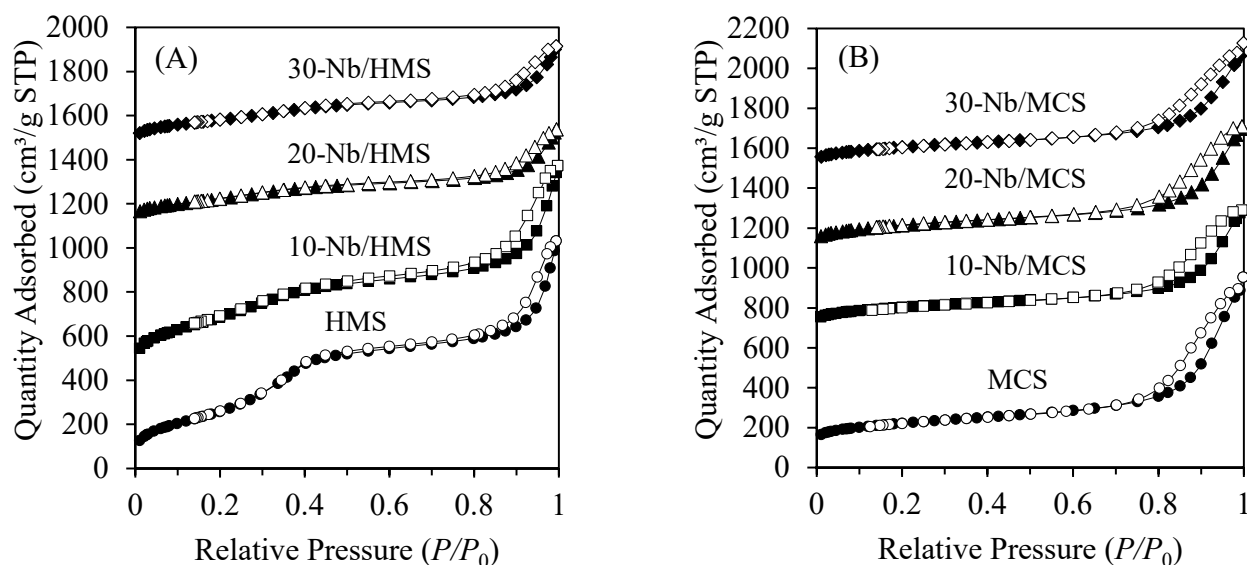

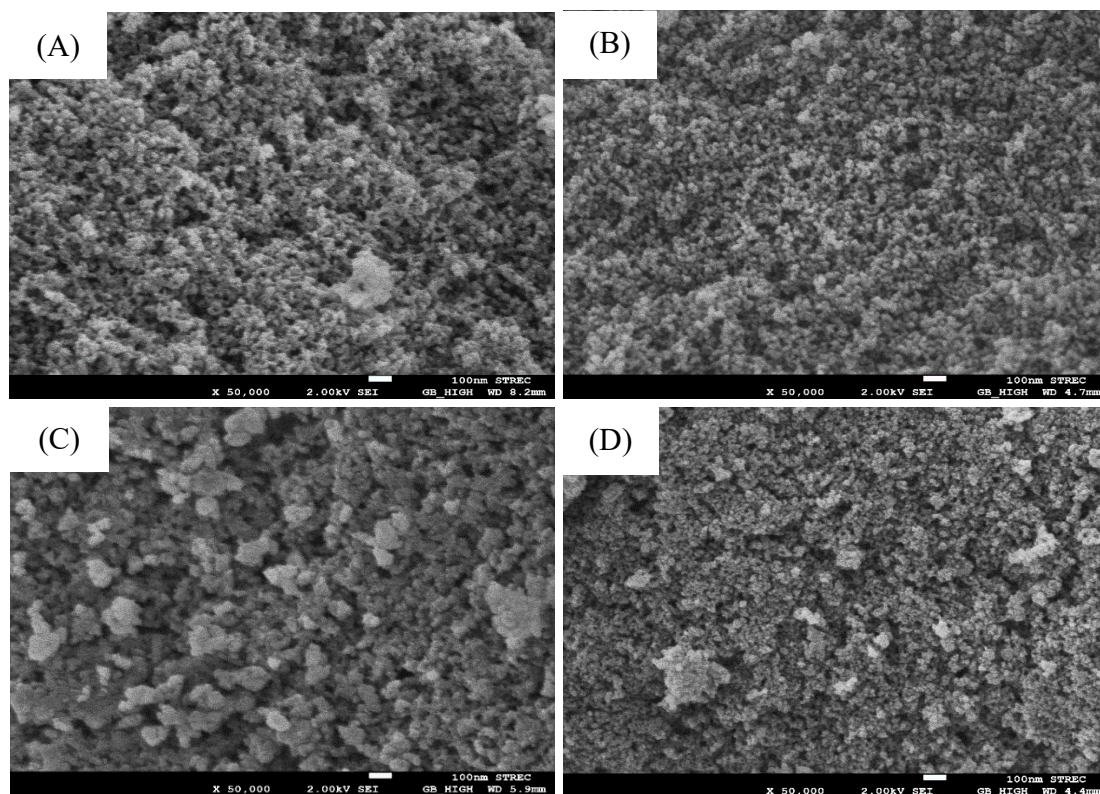**Figure 3.** N$_2$ physisorption isotherms of (**A**) *x*-Nb/HMS and (**B**) *x*-Nb/MCS catalysts.

Figure 4. FE-SEM images of (**A**) HMS, (**B**) MCS, (**C**) 10-Nb/HMS, and (**D**) 10-Nb/MCS at magnification of 50,000×.

Table 1. Physicochemical and acid properties of HMS and MCS with different Nb loading amount.

Catalyst.	Crystallite Size (nm) [a]	S_{BET} (m² g⁻¹) [b]	D_p (nm) [c]	V_t (cm³ g⁻¹) [d]	Acid Sites Distribution (μmol g⁻¹) [e]				Type of Acid Sites (μmol g⁻¹) [f]		
					W	M	S	Total	B	L	B/L Ratio
HMS	n.d.	1066	2.7	1.6	96.4	0.0	0.0	96.4	0.0	40.1	0.0
10-Nb/HMS	n.d.	1052	2.5	1.5	185.9	59.8	0.0	245.6	29.9	72.4	0.4
20-Nb/HMS	39.7	475	2.3	0.7	n.d.	n.d.	n.d.	n.d.	n.d.	n.d.	n.d.
30-Nb/HMS	47.4	489	2.3	0.7	n.d.	n.d.	n.d.	n.d.	n.d.	n.d.	n.d.
NR/HMS	n.d.	740	2.3	1.4	n.d.	n.d.	n.d.	n.d.	n.d.	n.d.	n.d.
MCS	n.d.	413	2.1	1.3	47.7	0.0	0.0	47.7	0.0	11.0	0.0
10-Nb/MCS	n.d.	404	2.0	1.1	101.5	24.1	9.3	134.9	15.0	12.9	1.2
20-Nb/MCS	45.8	407	1.9	1.0	93.7	39.6	0.0	133.3	13.2	10.3	1.3
30-Nb/MCS	49.0	375	1.7	0.9	66.0	52.6	0.0	118.6	12.3	7.1	1.7

[a] Crystallite size of Nb_2O_5 determined from XRD using Scherrer's equation at $2\theta = 22.6°$. [b] BET surface area. [c] BJH pore diameter. [d] Total pore volume. [e] Determined from NH_3-TPD: W = weak acid sites (50–200 °C), M = medium acid sites (200–300 °C) and S = strong acid sites (>300 °C). [f] Determined from Py-FTIR: B = Brønsted acid sites and L = Lewis acid sites.

The temperature-programmed desorption of NH_3 (NH_3-TPD) profiles of representative HMS and MCS catalysts are compared in Figure S3 (SM). The acid sites of Nb/HMS and Nb/MCS catalysts were classified into three types, corresponding to three ranges of desorption temperatures. The desorption occurred at 50–200 °C and was assigned to the acid sites weakly adsorbed NH_3, such as silanol groups (Si–OH) on the HMS and MCS surface, and hydroxide groups of Nb (Nb–OH) [10]. The medium acid sites were related to the desorption of NH_3 at 200–300 °C, which were attributed to Lewis acid character of Nb^{5+} in the oxide crystals (Nb–O) [12]. The desorption above 300 °C was designated to strong Lewis acid sites, as the Nb^{5+} species on the edges and corners of the oxide crystals. As shown in Table 1, MCS had a lower amount of weak acid sites than HMS due to a smaller number of Si–OH groups on the nanocomposite surface. The Nb impregnation not only increased the content of weak acidity but also generated the medium acid sites. The smaller Nb_2O_5 crystallites on the HMS surface should contribute to the higher total acidity of 10-Nb/HMS than 10-Nb/MCS [33]. With increasing the Nb loading amount on MCS, the weak acidity was decreased, while the content of medium acid sites increased. It was explained by an enlarged crystallite size of Nb_2O_5 as evidenced by the XRD and TEM analysis.

The amount of Brønsted and Lewis acid sites in the catalysts was determined by in situ Fourier transform infrared spectroscopy using pyridine as probe molecule (Py-FTIR). As revealed in Figure 5, the bands at 1445 and 1595 cm⁻¹ were assigned to the pyridine molecules adsorbed on weakly acidic groups (Si–OH and oxygen functional groups on the carbon surface). The bands at 1450, 1607 and 1623 cm⁻¹ were attributed to the pyridine molecules coordinated with Lewis acid sites, while the bands at 1540 and 1640 cm⁻¹ were corresponded to the pyridinium ions (PyH⁺) adsorbed on Brønsted acid sites [34]. The superposition of bands related to the adsorbed pyridine on both Brønsted and Lewis acid sites was present at 1490 cm⁻¹. The parent HMS and MCS materials exhibited the absence of Brønsted acidity [35]. After the Nb impregnation, the bands related to weakly acidic sites were decreased, which indicated the deposition of Nb_2O_5 on the surface of HMS and MCS. The amount of Brønsted and Lewis acid sites as calculated from the Py-FTIR spectra is reported in Table 1. With increasing the Nb loading, the total acidity was decreased. It is explained by an enlarged crystallite size as indicated by the XRD result (Figure 2). Ekhsan et al. [10] reported that Lewis acid sites were originated from $Nb^{\delta+}$ ions, while Brønsted acidity was generated from bridging Nb–OH–Nb species. At a high Nb concentration, an increased interaction between the isolate Nb species and their nearest neighbors resulted in an enhanced formation of Nb–O–Nb bonds, which mainly reduced the content of $Nb^{\delta+}$ ions [12]. Consequently, the B/L ratio was increased with increasing the Nb content.
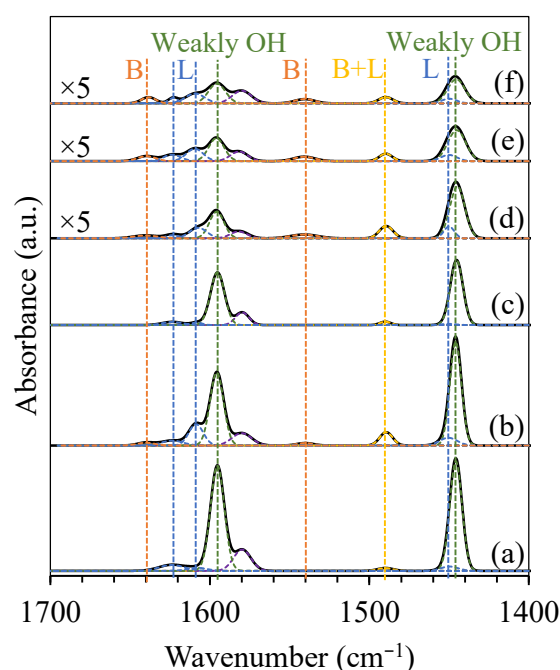
Figure 5. Py-FTIR spectra of (**a**) HMS, (**b**) 10-Nb/HMS, (**c**) MCS, (**d**) 10-Nb/MCS, (**e**) 20-Nb/MCS, and (**f**) 30-Nb/MCS catalysts.

2.2. Catalytic Performance of Nb/HMS and Nb/MCS Catalysts

2.2.1. Catalysts Screening

The glucose conversion into HMF was studied over HMS and MCS with different Nb loading levels as shown in Table 2. The possible reaction pathway for catalytic conversion of glucose into HMF in the present study is illustrated in Scheme 1. The glucose conversion increased around 10% over 10-Nb/HMS and 10-Nb/MCS catalysts due to an increased amount of total acid sites (Table 1). Besides, MCS and 10-Nb/MCS not only exhibited higher HMF yield and selectivity but also a lower humins yield than HMS and 10-Nb/HMS. This result was in accord with the previous work, which indicated the beneficial effect of catalyst hydrophobicity on the HMF formation [14]. Zhu et al. [36] reported that HMF was rehydrated to 2,5-dioxo-6-hydroxyhexanal (DHH), which was thermodynamically unstable intermediate in the reaction system consisting of water and acid catalyst. Therefore, the hydrophobicity of MCS retarded the condensation of DHH as a monomer for humins growth [37,38].

When the Nb concentration on MCS was increased from 10 to 20 and 30 wt.%, the glucose conversion and HMF yield were slightly decreased due to a decreased acidity (Table 1) [13]. Li et al. [5] reported that, at a high B/L ratio (0.9−1.7), the HMF yield was decreased since the humins formation was promoted over Brønsted acid sites via aldol addition and condensation of HMF [39]. Over the catalyst with a high Lewis acidity, the formation of humins was facilitated via polymerization of glucose, fructose, and HMF [40]. Thus, a balance of B/L ratio was necessary for selective conversion of glucose into HMF. In addition, the Nb/MCS catalysts provided a low furfural yield (less than 1%). It was demonstrated that the glucose molecules tended to convert to HMF, rather than pentose as an intermediate for furfural formation, via dehydration under the combined catalysis of Lewis and Brønsted acid sites [41]. The highest HMF yield of 35.0% was obtained over 10-Nb/MCS at 78.9% glucose conversion at 170 °C for 1 h. Hereafter, 10-Nb/MCS as a suitable catalyst was used for optimizing the reaction conditions for HMF synthesis.

Table 2. Glucose conversion and products distribution obtained from glucose conversion [a] over the HMS and MCS catalysts with different Nb loading amount.

Catalyst	Glucose Conversion (%)	Yield (%)				HMF Selectivity (%)
		Fructose	HMF	Furfural	Others [b]	
HMS	68.9 ± 0.6	3.8 ± 0.3	30.2 ± 0.7	0.3 ± 0.0	34.6 ± 0.2	43.9 ± 0.6
10-Nb/HMS	78.6 ± 0.8	4.3 ± 0.1	29.4 ± 0.8	0.6 ± 0.0	44.3 ± 1.6	37.4 ± 1.4
20-Nb/HMS	74.3 ± 1.0	5.4 ± 0.1	27.0 ± 0.8	0.4 ± 0.0	41.5 ± 1.7	36.3 ± 1.6
30-Nb/HMS	68.0 ± 0.8	8.1 ± 0.4	24.1 ± 0.5	0.3 ± 0.0	35.5 ± 0.7	35.5 ± 0.3
MCS	69.2 ± 0.6	5.4 ± 0.3	32.5 ± 0.5	0.3 ± 0.0	31.1 ± 0.4	47.0 ± 0.3
10-Nb/MCS	78.9 ± 0.7	4.8 ± 0.5	35.0 ± 1.0	0.6 ± 0.1	38.6 ± 1.1	44.3 ± 1.5
20-Nb/MCS	78.1 ± 0.2	5.0 ± 0.0	30.0 ± 0.9	0.5 ± 0.0	42.5 ± 0.7	38.5 ± 1.0
30-Nb/MCS	76.6 ± 0.8	5.1 ± 0.0	28.4 ± 0.9	0.5 ± 0.0	42.7 ± 0.4	37.0 ± 1.1

[a] Reaction conditions: Catalyst amount, 0.1 g; glucose concentration, 0.07 M; solvent volume (1:2 *v/v* water saturated with NaCl: THF), 30 mL; temperature, 170 °C; time, 1 h; N_2 pressure, 10 bar. [b] Others are mainly humins.
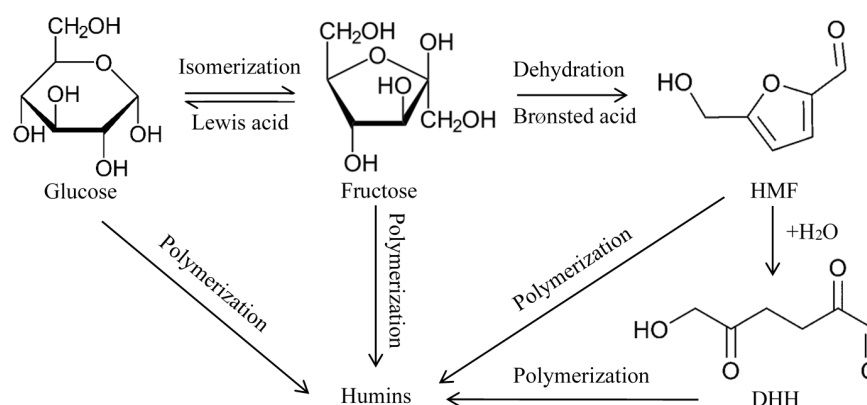
Scheme 1. The reaction pathway for the conversion of glucose into HMF.

2.2.2. Effect of Reaction Conditions on Glucose Conversion over10-Nb/MCS Catalyst

Figure 6 shows the effect of reaction temperature and time on the glucose conversion and products distribution over 10-Nb/MCS. The glucose conversion was increased with reaction temperature (Figure 6A) because the main catalytic reactions (isomerization and dehydration) in this system are endothermic nature [42]. The fructose concentration was observed at low concentration in all experiments, which suggested a high affinity of catalyst surface with fructose molecule, as well as a fast dehydration and/or condensation of fructose to other products (Figure 6B). The maximum HMF yield was a function of reaction time as shown in Figure 6C. At 190 °C, the HMF yield increased to the maximum value within 1 h, and then decreased when the reaction time was extended to 4 h. Hirano et al. [43] reported that a decrease in the HMF yield with increasing reaction time was explained by the propensity of humins formation via polymerization of glucose, fructose, HMF, and other reactive intermediates. This result was consistent with an increased humins yield with prolonged reaction time (Figure 6D). The suitable conditions for HMF synthesis over 10-Nb/MCS were 30 wt.% catalyst loading at 190 °C for 1 h, giving the highest HMF yield of 51.3% at 98.5% glucose conversion.

Effect of catalyst loading level on the glucose conversion, HMF yield, and humins yield in the presence of 10-Nb/MCS is shown in Figure 7. When the amount of catalyst was increased, the glucose conversion was gradually increased and near completion at a 30 wt.% loading level. However, the HMF yield decreased concomitantly with an enhanced humins formation. It was attributed to an excess amount of Brønsted and Lewis acid sites available in the reaction system, which not only promoted the glucose dehydration into HMF but also the condensation of formed HMF to humins. The observed result was in accord with the previous work by Guo et al. [44]. At the catalyst loading of 5 wt.%, the highest HMF yield (57.5%) was achieved at 93.2% glucose conversion.
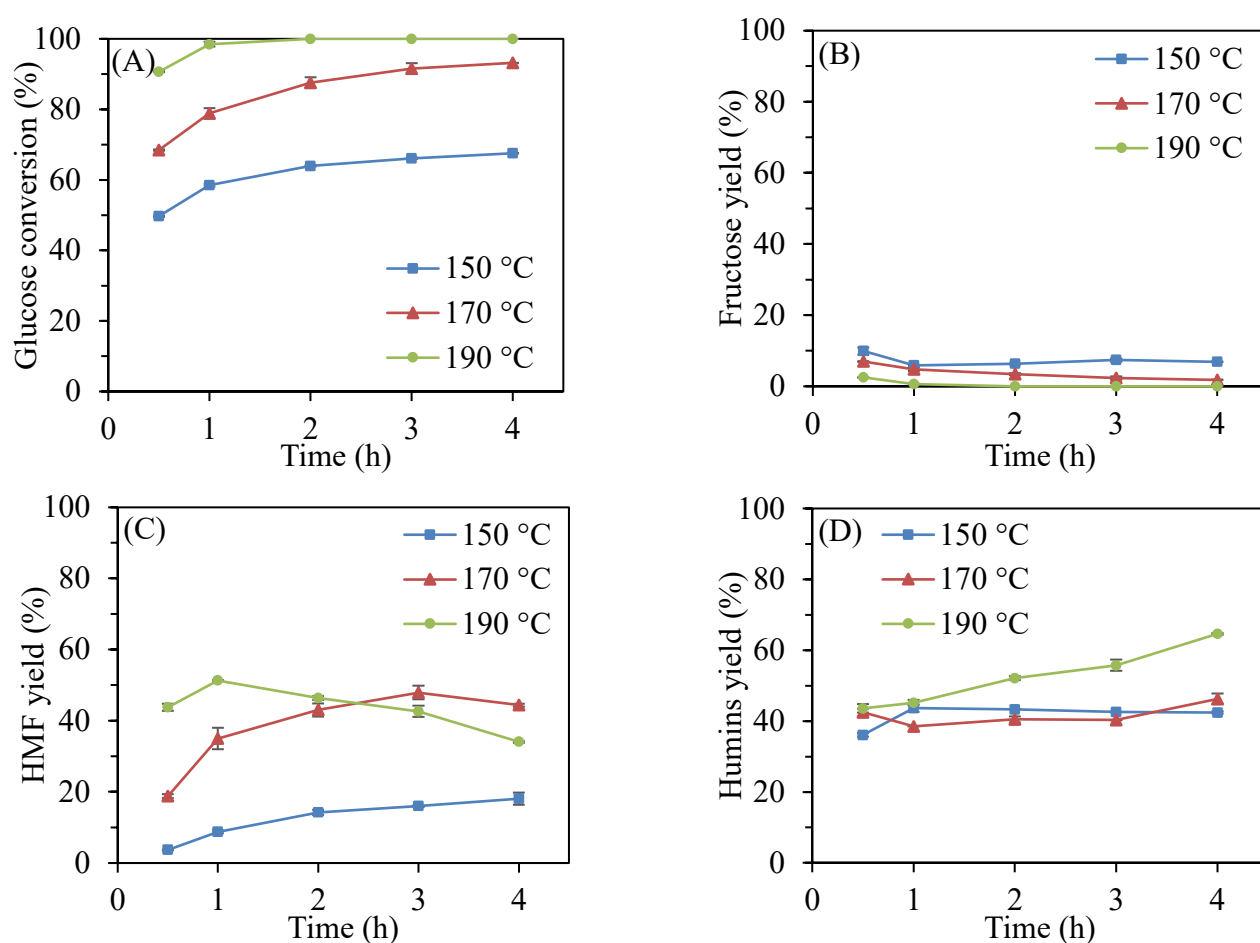
Figure 6. Effect of reaction temperature and time on (**A**) glucose conversion, (**B**) fructose yield, (**C**) HMF yield, and (**D**) humins yield using 10-Nb/MCS catalyst. (Reaction conditions: Catalyst amount, 0.1 g; glucose concentration, 0.07 M; solvent volume (1:2 *v/v* water saturated with NaCl: THF), 30 mL; N$_2$ pressure, 10 bar).
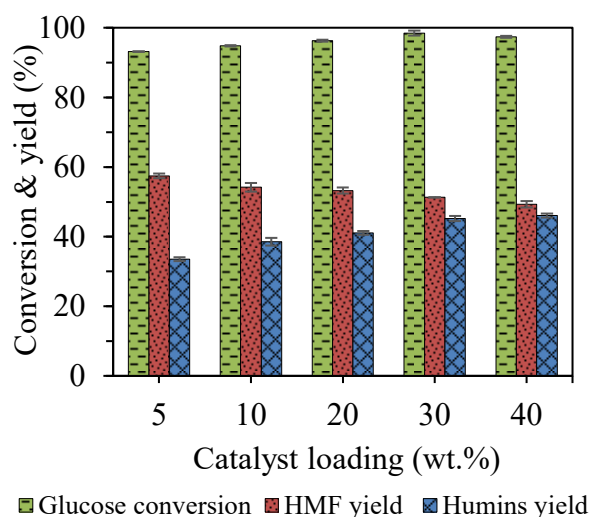

Figure 7. Effect of amount of 10-Nb/MCS catalyst loading on glucose conversion, HMF yield and humins yield. (Reaction conditions: glucose concentration, 0.07 M; solvent volume (1:2 *v/v* water saturated with NaCl: THF), 30 mL; temperature, 190 °C; time, 1 h; N$_2$ pressure, 10 bar).

2.2.3. Catalyst Reusability

Hydrothermal stability of catalytic materials is of great importance for successful development of heterogeneously catalyzed conversion of biomass-derived carbohydrates to value-added chemical products in aqueous solution. Herein, we verified the stability of 10-Nb/MCS as the suitable catalyst in the HMF synthesis from glucose via a reusability study. After thoroughly washing with deionized water and THF, the spent 10-Nb/MCS was calcined at 550 °C for 5 h under Ar flow prior to reuse in the glucose conversion. The reaction was operated under the suitable conditions as described in the previous sections. The reusability of this catalyst is shown in Figure 8. It can be seen that no significant loss of glucose conversion, and the HMF yield of >57% retained in five repetitive uses. Moreover, the humins yield was insignificantly changed. Nb_2O_5 is an acidic oxide with excellent hydrothermal stability in the aqueous-phase reaction systems [11–13]. The carbon moieties dispersed in the MCS nanocomposites offered hydrophobic properties [23], and so retarded the adsorption of H_2O on the catalyst surface. The overall results indicated that 10-Nb/MCS not only had good catalytic activity, but also high hydrothermal stability, in the selective synthesis of HMF from an aqueous glucose solution.
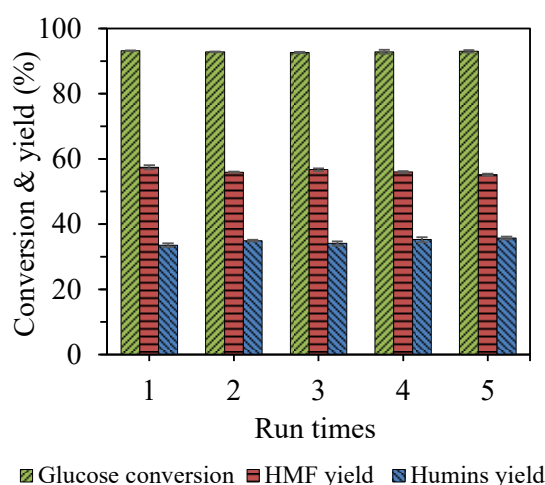

Figure 8. Reusability of 10-Nb/MCS in catalytic conversion of glucose into HMF. (Reaction conditions: Catalyst amount, 0.018 g; glucose concentration, 0.07 M; solvent volume (1:2 *v/v* water saturated with NaCl: THF), 30 mL; temperature, 190 °C; time, 1 h; N_2 pressure, 10 bar).

3. Experimental

3.1. Material and Chemical Reagents

Natural rubber (NR, technically specified STR-5L grade) was supplied by the Thai Hua Chumporn Natural Rubber Co., Ltd. (Bangkok, Thailand). Tetraethyl orthosilicate (TEOS, AR grade, 99%), dodecylamine (DDA, AR grade, 98%), ammonium niobite (V) oxalate hydrate (99.99%), and 2,5-furandicarboxylic acid (FDCA, AR grade, 97%) were purchased from Sigma Aldrich (Selangor, Malaysia). Tetrahydrofuran (THF, AR grade, 99.5%), sulfuric acid (H_2SO_4, AR grade, 98%), and methyl ethyl ketone (MEK, AR grade, 99.5%) were obtained from QRëC (Bangkok, Thailand). Ethanol (AR grade, 99.5%) was supplied by Merck (Bangkok, Thailand). *D*-Glucose (AR grade, >99%) was purchased from Ajax Finechem (Bangkok, Thailand), while sodium chloride (NaCl, AR grade, >99%) was supplied by J.T.Baker (Bangkok, Thailand).

3.2. Synthesis of Pure Silica HMS

HMS was synthesized via a sol-gel process using THF as a co-solvent, TEOS as a silica precursor, and DDA as an organic template, as reported previously [20]. Typically, DDA was dissolved in a solution of THF and deionized water under stirring. TEOS was then added dropwise into this solution, and the resulting gel with a molar composition of

0.05 TEOS: 0.02 DDA: 2.94 H_2O: 0.18 THF was stirred at ambient temperature for 30 min. After aging at 40 °C for 24 h, the white solid was recovered by filtration and drying at 60 °C for 18 h. The amine template was removed by extraction with 0.05 M H_2SO_4/ethanol at 80 °C for 4 h. The final product was thoroughly washed with ethanol and dried at 60 °C overnight.

3.3. Synthesis of MCS Nanocomposite

An NR/HMS nanocomposite prepared via an in situ sol-gel method was used as a precursor for the synthesis of MCS material [21,22,45]. Typically, 0.5 g of NR sheet was swollen in TEOS at room temperature for 16 h, and then dissolved in THF under stirring overnight. To this solution, DDA and additional TEOS were added dropwise. After stirring at ambient temperature for 30 min, deionized water was slowly added to the mixture. The resulting gel with a molar composition of 0.05 TEOS: 0.02 DDA: 2.94 H_2O: 0.55 THF: 0.007 NR was aged at 40 °C for 72 h. The white slurry was precipitated in 50 mL of ethanol, and then the solid product was filtered and dried at 60 °C for 18 h. Finally, the organic template was removed by extraction with 2 M H_2SO_4/ethanol at 80 °C for 4 h, followed by washing with ethanol and drying at 60 °C for 24 h. The MCS nanocomposite was achieved by carbonization of NR/HMS precursor at 700 °C for 1 h under argon (Ar) atmosphere.

3.4. Synthesis of Niobium Oxides Supported on HMS (Nb/HMS) and MCS (Nb/MCS)

Nb/HMS and Nb/MCS with different Nb loading amounts (10, 20, and 30 wt.%) were prepared by an incipient wetness impregnation, where ammonium niobite(V) oxalate hydrate was used as the Nb precursor. The required amount of Nb precursor was completely dissolved in the predetermined amount of deionized water. The resulting solution was added dropwise onto the dried HMS and MCS powder under stirring. Subsequently, the wet powder was dried at 60 °C for 24 h. The materials were finally calcined under Ar flow at 550 °C for 5 h. The obtained catalysts were designed as *x*-Nb/HMS and *x*-Nb/MCS, where *x* represents the Nb loading amount of 10, 20, and 30 wt.%.

3.5. Catalysts Characterization

The thermal decomposition pattern and carbon content of nanocomposites were determined by TG/DTA using a Rigaku Thermo plus TG 8120 instrument (Tokyo, Japan). The analysis was performed at a heating rate of 10 °C min^{-1} from 50 °C to 1000 °C under dry air flow of 50 mL min^{-1}. The surface functional groups of materials were determined by XPS using an ESCA 1700R system (ULVAC-PHI, Inc., Kanagawa, Japan) with Al Kα radiation (1486.8 eV). The binding energy (BE) for the high-resolution C1s spectrum was calibrated by setting C1s at 284.6 eV. The curve-fitting of XPS spectra was performed with the OriginPro 8.5 software version 85E (OriginLab Corporation, Northampton, MA, USA).

The structural information of the materials was obtained from powder XRD analysis using a Bruker D8 ADVANCE diffractometer (Bruker Corporation, Billerica, MA, USA) equipped with a Cu Kα radiation (λ = 1.5406 Å), which was operated at voltage of 40 kV and current of 40 mA. The XRD patterns were recorded at room temperature over the 2θ range of 5–80° with a scanning step of 0.02° and a count time of 1 s. The textural properties of the template-free materials were determined by N_2 physisorption measurement at −196 °C using a Micromeritics ASAP 2020 surface area and porosity analyzer (Micromeritics Instrument Corporation, Norcross, GA, USA). The sample was degassed at 150 °C for 2 h prior to the measurement. The specific surface area (S_{BET}) was calculated from adsorption data in the relative pressure (P/P_0) range from 0.05 to 0.3 using the Brunauer-Emmett-Teller (BET) equation. The total pore volume (V_t) was obtained from the adsorption branch at $P/P_0 \approx 0.99$. The Barret-Joyner-Halenda (BJH) plot was applied to determine pore size (D_p) using the adsorption data.

The acidic properties of calcined catalysts were examined by NH_3-TPD using a Micromeritics AutoChemII 2920 chemisorption analyzer (Georgia, USA). Prior to the analysis, the sample powder was pretreated at 500 °C for 60 min under a helium (He) flow

(50 mL min^{-1}). Subsequently, 10% NH_3 in He gas (10 mL min^{-1}) was introduced to the sample at 50 °C for 30 min to allow the adsorption of NH_3. The physisorbed gas was flushed, and the sample was heated under a He flow (50 mL min^{-1}) to 500 °C at a heating rate of 10 °C min^{-1} to desorb NH_3. The total amount and distribution of acid sites were determined after deconvolution of TPD profiles using OriginPro 8.5 software version 85E (OriginLab Corporation, Northampton, MA, USA).

The in situ Py-FTIR analysis was performed on a NICOLET iS10 FTIR spectrometer (Thermo Fisher Scientific, Waltham, MA, USA). The powdery sample was pressed into a self-supporting disc and placed in a quartz cell equipped with CaF_2 windows. The sample disc was pretreated at 500 °C for 1 h under vacuum to remove some impurities. After cooling to 50 °C, pyridine vapor was introduced into the cell until the adsorption reached equilibrium, followed by evacuating at the same temperature for 15 min. The spectra were recorded for 96 scans. The corresponding bands were deconvoluted for better assignment using OriginPro 8.5 software version 85E (OriginLab Corporation, Northampton, MA, USA), and the content of both acid sites was quantified using extinction coefficients.

The morphological study was performed by FE-SEM using a JEOL JSM-7610F instrument (JEOL Ltd., Tokyo, Japan) operating at 40 kV. The sample powder was dispersed on carbon tape, followed by gold coating. The FE-SEM images were recorded at magnification of 50,000×. TEM was used to investigate the dispersion of Nb crystallites. The TEM images (200,000× magnification) were collected on a JEOL JEM-2100 Plus transmission electron microscope (Tokyo, Japan) operating at accelerating voltage of 200 kV.

3.6. Catalytic Conversion of Glucose into HMF

The catalytic dehydration of glucose to HMF was carried out in a 50-mL stainless-steel autoclave. The reaction temperature was controlled by an oil bath, and the reaction mixture was agitated using a magnetic stirrer. In a typical reaction, 0.36 g of glucose was completely dissolved in a biphasic solvent with a volume ratio of THF: H_2O (saturated with NaCl) of 2:1, corresponding to the glucose concentration of 0.07 M, and then poured into the autoclave. Subsequently, a required amount of catalyst was put in the reactor. After tightly sealing the autoclave cover, the reactor was pressurized with 10 bar N_2 gas to keep the solvent in liquid state. When the mixture temperature was raised to the desired set point, zero time was recorded. After the reaction course, the mixture was cooled down to room temperature using an ice bath, followed by centrifugation to remove the solid catalyst. The liquid product was taken using a syringe filter for composition analysis. The spent catalyst was washed with deionized water and THF sequentially and dried at 60 °C overnight. Before being reused, the spent catalyst was activated by calcination at 550 °C for 5 h under Ar flow.

3.7. Products Analysis

The liquid product was analyzed by high-performance liquid chromatography (HPLC) using a Shimadzu LC-10ADvp apparatus (Kyoto, Japan) equipped with a Bio-Rad Aminex HPX-87H column (Aminex Corporation, Santa Monica, CA, USA). Two types of detectors, i.e., a refractive index detector and an ultraviolet detector at 240 nm, were used for analysis of aqueous and organic phase, respectively. The mobile phase was 0.005 M H_2SO_4 solution with a flow rate of 0.7 mL min^{-1}. The column temperature was maintained at 60 °C. The glucose conversion and products yield were calculated according to an internal standardization method using FDCA as a reference standard.

4. Conclusions

In summary, we have successfully synthesized the Nb/MCS catalysts by which MCS was prepared from the NR/HMS nanocomposite via carbonization, and Nb_2O_5 was loaded onto MCS via incipient wetness impregnation, followed by calcination at 550 °C. The characterization results indicate that 10-Nb/MCS not only had good textural properties but also a high dispersion of Nb_2O_5 crystallites on the MCS surface. By varying the

Nb loading level, the molar ratio of Brønsted/Lewis acid sites could be optimized. The 10-Nb/MCS catalyst showed a good performance in the conversion of glucose into HMF in a biphasic water-THF solvent, achieving the highest HMF yield of 57.9% at 93.2% glucose conversion, when the reaction was carried out using 0.018 g catalyst loading at 190 °C for 1 h. Furthermore, 10-Nb/MCS exhibited a high catalytic stability in the HMF synthesis from glucose in the biphasic solvent since it could be reused at least five times without a significant loss of activity. Its superior performance was ascribed to the suitable Brønsted/Lewis acidity ratio (1.2), and the hydrophobic properties generated from the carbon moieties dispersed in the MCS nanocomposite. The overall results suggest a potential application of NR as a low-cost and sustainable carbon source in the preparation of high surface area and hydrophobic MCS support, and a practical use of 10-Nb/MCS in the acid-catalyzed conversion of glucose into HMF at a high concentration of glucose substrate.

Supplementary Materials: The following are available online at https://www.mdpi.com/article/10.3390/catal11080887/s1, Figure S1: Weight loss and DTA curves of pure silica HMS and MCS nanocomposite, Figure S2: C1s XPS spectrum of MCS nanocomposite, Figure S3: NH_3-TPD profiles of HMS and MCS with different Nb loading amount.

Author Contributions: R.K.: Investigation, validation, and writing—original draft; S.Y.: Methodology, validation, writing—review and editing; C.N.: Conceptualization, funding acquisition, supervision, and writing—review and editing. All authors have read and agreed to the published version of the manuscript.

Data Availability Statement: The data presented in this study are available in the article and the Supplementary Data.

Conflicts of Interest: The authors declare that they have no known competing financial interests or personal relationships that could have appeared to influence the work reported in this paper.

References

1. Qiu, G.; Huang, C.; Sun, X.; Chen, B. Highly active niobium-loaded montmorillonite catalysts for the production of 5-hydroxymethylfurfural from glucose. *Green Chem.* **2019**, *21*, 3930–3939. [CrossRef]
2. Saravanan, K.; Park, K.S.; Jeon, S.; Bae, J.W. Aqueous phase synthesis of 5-hydroxymethylfurfural from glucose over large pore mesoporous zirconium phosphates: Effect of calcination temperature. *ACS Omega* **2018**, *3*, 808–820. [CrossRef] [PubMed]
3. Shirai, H.; Ikeda, S.; Qian, E.W. One-pot production of 5-hydroxymethylfurfural from cellulose using solid acid catalysts. *Fuel Process. Technol.* **2017**, *159*, 280–286. [CrossRef]
4. Hu, L.; Lin, L.; Wu, Z.; Zhou, S.; Liu, S. Chemocatalytic hydrolysis of cellulose into glucose over solid acid catalysts. *Appl. Catal. B Environ.* **2015**, *174*, 225–243. [CrossRef]
5. Li, X.; Peng, K.; Xia, Q.; Liu, X.; Wang, Y. Efficient conversion of cellulose into 5-hydroxymethylfurfural over niobia/carbon composites. *Chem. Eng. J.* **2018**, *332*, 528–536. [CrossRef]
6. Candu, N.; Fergani, M.; Verziu, M.; Cojocaru, B.; Jurca, B.; Apostol, N.; Teodorescu, C.; Parvulescu, V.I.; Coman, S.M. Efficient glucose dehydration to HMF onto Nb-BEA catalysts. *Catal. Today* **2019**, *325*, 109–116. [CrossRef]
7. Perez, G.P.; Mukherjee, A.; Dumont, M.-J. Insights into HMF catalysis. *J. Ind. Eng. Chem.* **2019**, *70*, 1–34. [CrossRef]
8. Vieira, J.L.; Almeida-Trapp, M.; Mithöfer, A.; Plass, W.; Gallo, J.M.R. Rationalizing the conversion of glucose and xylose catalyzed by a combination of Lewis and Brønsted acids. *Catal. Today* **2020**, *344*, 92–101. [CrossRef]
9. Zhu, L.; Wang, J.; Zhao, P.; Song, F.; Sun, X.; Wang, L.; Cui, H.; Yi, W. Preparation of the Nb-P/SBA-15 catalyst and its performance in the dehydration of fructose to 5-hydroxymethylfurfural. *J. Fuel Chem. Technol.* **2017**, *45*, 651–659. [CrossRef]
10. Ekhsan, J.M.; Lee, S.L.; Nur, H. Niobium oxide and phosphoric acid impregnated silica–titania as oxidative-acidic bifunctional catalyst. *Appl. Catal. A Gen.* **2014**, *471*, 142–148. [CrossRef]

11. Carniti, P.; Gervasini, A.; Marzo, M. Absence of expected side-reactions in the dehydration reaction of fructose to HMF in water over niobic acid catalyst. *Catal. Commun.* **2011**, *12*, 1122–1126. [CrossRef]

12. Jiao, H.; Zhao, X.; Lv, C.; Wang, Y.; Yang, D.; Li, Z.; Yao, X. Nb_2O_5-γ-Al_2O_3 nanofibers as heterogeneous catalysts for efficient conversion of glucose to 5-hydroxymethylfurfural. *Sci. Rep.* **2016**, *6*, 1–9. [CrossRef] [PubMed]

13. Peng, K.; Li, X.; Liu, X.; Wang, Y. Hydrothermally stable Nb-SBA-15 catalysts applied in carbohydrate conversion to 5-hydroxymethylfurfural. *Mol. Catal.* **2017**, *441*, 72–80. [CrossRef]

14. Lin, F.; Wang, K.; Gao, L.; Guo, X. Efficient conversion of fructose to 5-hydroxymethylfurfural by functionalized γ-Al_2O_3 beads. *Appl. Organomet. Chem.* **2019**, *33*, 1–13. [CrossRef]

15. Yang, G.; Wang, C.; Lyu, G.; Lucia, L.; Chen, J. Catalysis of glucose to 5-hydroxymethylfurfural using Sn-beta zeolites and a Brønsted acid in biphasic systems. *BioResources* **2015**, *10*, 5863–5875. [CrossRef]

16. Hu, L.; Tang, X.; Wu, Z.; Lin, L.; Xu, J.; Xu, N.; Dai, B. Magnetic lignin-derived carbonaceous catalyst for the dehydration of fructose into 5-hydroxymethylfurfural in dimethylsulfoxide. *Chem. Eng. J.* **2015**, *263*, 299–308. [CrossRef]

17. Zhong, R.; Peng, L.; de Clippel, F.; Gommes, C.; Goderis, B.; Ke, X.; Tendeloo, G.V.; Jacobs, P.A.; Sels, B.F. An eco-friendly soft template synthesis of mesostructured silica-carbon nanocomposites for acid catalysis. *ChemCatChem* **2015**, *7*, 3047–3058. [CrossRef]

18. Zhong, R.; Sels, B.F. Sulfonated mesoporous carbon and silica-carbon nanocomposites for biomass conversion. *Appl. Catal. B Environ.* **2018**, *236*, 518–545. [CrossRef]

19. Vaysse, L.; Bonfils, F.; Sainte-Beuve, J.; Cartault, M. 10.1. 7-Natural rubber. In *Polymer Sci-ence: A Comprehensive Reference. Polymers for a Sustainable Environment and Green Energy*; McGrath, J.E., Hickner, M.A., H öfer, R., Eds.; Elsevier: Amsterdam, The Netherlands, 2012; p. 281.

20. Chaowamalee, S.; Ngamcharussrivichai, C. Facile fabrication of mesostructured natural rubber/silica nanocomposites with enhanced thermal stability and hydrophobicity. *Nanoscale Res. Lett.* **2019**, *14*, 1–13. [CrossRef] [PubMed]

21. Nuntang, S.; Yousatit, S.; Chaowamalee, S.; Yokoi, T.; Tatsumi, T.; Ngamcharussrivichai, C. Mesostructured natural rubber/*in situ* formed silica nanocomposites: A simple way to prepare mesoporous silica with hydrophobic properties. *Microporous Mesoporous Mater.* **2018**, *259*, 79–88. [CrossRef]

22. Nuntang, S.; Yousatit, S.; Yokoi, T.; Ngamcharussrivichai, C. Tunable mesoporosity and hydrophobicity of natural rubber/hexagonal mesoporous silica nanocomposites. *Microporous Mesoporous Mater.* **2019**, *275*, 235–243. [CrossRef]

23. Yousatit, S.; Pitayachinchot, H.; Wijitrat, A.; Chaowamalee, S.; Nuntang, S.; Soontaranon, S.; Rugmai, S.; Yokoi, T.; Ngamcharussrivichai, C. Natural rubber as a renewable carbon source for mesoporous carbon/silica nanocomposites. *Sci. Rep.* **2020**, *10*, 1–14. [CrossRef]

24. Farani, M.R.; Parsi, P.K.; Riazi, G.; Ardestani, M.S.; Rad, H.S. Extending the application of a magnetic PEG three-part drug release device on a graphene substrate for the removal of Gram-positive and Gram-negative bacteria and cancerous and pathologic cells. *Drug Des. Dev. Ther.* **2019**, *13*, 1581. [CrossRef] [PubMed]

25. Johra, F.T.; Jung, W.-G. Hydrothermally reduced graphene oxide as a supercapacitor. *Appl. Surf. Sci.* **2015**, *357*, 1911–1914. [CrossRef]

26. Nie, H.; Fu, L.; Zhu, J.; Yang, W.; Li, D.; Zhou, L. Excellent tribological properties of lower reduced graphene oxide content copper composite by using a one-step reduction molecular-level mixing process. *Materials* **2018**, *11*, 600. [CrossRef] [PubMed]

27. Baharudin, K.B.; Taufiq-Yap, Y.H.; Hunns, J.; Isaacs, M.; Wilson, K.; Derawi, D. Mesoporous NiO/Al-SBA-15 catalysts for solvent-free deoxygenation of palm fatty acid distillate. *Microporous Mesoporous Mater.* **2019**, *276*, 13–22. [CrossRef]

28. Jabeen, B.; Rafique, U. Synthesis and application of metal doped silica particles for adsorptive desulphurization of fuels. *Environ. Eng. Res.* **2014**, *19*, 205–214. [CrossRef]

29. Liu, J.; Xue, D.; Li, K. Single-crystalline nanoporous Nb_2O_5 nanotubes. *Nanoscale Res. Lett.* **2011**, *6*, 1–8. [CrossRef]

30. Silva, A.; Wilson, K.; Lee, A.F.; Santos, V.C.; Bacilla, A.C.; Mantovani, K.M.; Nakagaki, S. Nb_2O_5/SBA-15 catalyzed propanoic acid esterification. *Appl. Catal. B Environ.* **2017**, *205*, 498–504. [CrossRef]

31. Przekop, R.E.; Kirszensztejn, P. Highly dispersed Pt on B_2O_3/Al_2O_3 support: Catalytic properties in the total oxidation of 1-butene. *React. Kinet. Mech. Catal.* **2016**, *118*, 325–335. [CrossRef]

32. Mandal, S.; Santra, C.; Kumar, R.; Pramanik, M.; Rahman, S.; Bhaumik, A.; Maity, S.; Sen, D.; Chowdhury, B. Niobium doped hexagonal mesoporous silica (HMS-X) catalyst for vapor phase Beckmann rearrangement reaction. *RSC Adv.* **2014**, *4*, 845–854. [CrossRef]

33. Ruiz, C.F.; Bedia, J.; Grau, J.M.; Romero, A.C.; Rodriguez, D.; Sainero, L.M. Promoting light hydrocarbons yield by catalytic hydrodechlorination of residual chloromethanes using palladium supported on zeolite catalysts. *Catalysts* **2020**, *10*, 1–17.

34. Penkova, A.; Bobadilla, L.F.; Romero-Sarria, F.; Centeno, M.A.; Odriozola, J.A. Pyridine adsorption on NiSn/MgO–Al_2O_3: An FTIR spectroscopic study of surface acidity. *Appl. Surf. Sci.* **2014**, *317*, 241–251. [CrossRef]

35. Umbarkar, S.; Biradar, A.; Mathew, S.; Shelke, S.; Malshe, K.; Patil, P.; Dagde, S.; Niphadkar, S.; Dongare, M. Vapor phase nitration of benzene using mesoporous MoO_3/SiO_2 solid acid catalyst. *Green Chem.* **2006**, *8*, 488–493. [CrossRef]

36. Zhu, L.; Fu, X.; Hu, Y.; Hu, C. Controlling the reaction networks for efficient conversion of glucose into 5-hydroxymethylfurfural. *ChemSusChem* **2020**, *13*, 4812–4832. [CrossRef]

37. Jung, D.; Körner, P.; Kruse, A. Kinetic study on the impact of acidity and acid concentration on the formation of 5-hydroxymethylfurfural (HMF), humins, and levulinic acid in the hydrothermal conversion of fructose. *Biomass Convers. Biorefinery* **2019**, *11*, 1155–1170. [CrossRef]
38. Patil, S.K.; Heltzel, J.; Lund, C.R. Comparison of structural features of humins formed catalytically from glucose, fructose, and 5-hydroxymethylfurfuraldehyde. *Energy Fuels* **2012**, *26*, 5281–5293. [CrossRef]
39. Li, X.; Peng, K.; Liu, X.; Xia, Q.; Wang, Y. Comprehensive understanding of the role of Brønsted and Lewis acid sites in glucose conversion into 5-hydromethylfurfural. *ChemCatChem* **2017**, *9*, 2739–2746. [CrossRef]
40. Swift, T.D.; Nguyen, H.; Anderko, A.; Nikolakis, V.; Vlachos, D.G. Tandem Lewis/Brønsted homogeneous acid catalysis: Conversion of glucose to 5-hydoxymethylfurfural in an aqueous chromium (III) chloride and hydrochloric acid solution. *Green Chem.* **2015**, *17*, 4725–4735. [CrossRef]
41. Li, W.; Xu, Z.; Zhang, T.; Li, G.; Jameel, H.; Chang, H.-m.; Ma, L. Catalytic conversion of biomass-derived carbohydrates into 5-hydroxymethylfurfural using a strong solid acid catalyst in aqueous γ-valerolactone. *BioResources* **2016**, *11*, 5839–5853. [CrossRef]
42. Takasaki, Y. Kinetic and equilibrium studies on D-glucose-D-fructose isomerization catalyzed by glucose isomerase from *Streptomyces* sp. *Agric. Biol. Chem.* **1967**, *31*, 309–313. [CrossRef]
43. Hirano, Y.; Beltramini, J.N.; Mori, A.; Nakamura, M.; Karim, M.R.; Kim, Y.; Nakamura, M.; Hayami, S. Microwave-assisted catalytic conversion of glucose to 5-hydroxymethylfurfural using "three dimensional" graphene oxide hybrid catalysts. *RSC Adv.* **2020**, *10*, 11727–11736. [CrossRef]
44. Guo, W.; Zuo, M.; Zhao, J.; Li, C.; Xu, Q.; Xu, C.; Wu, H.; Sun, Z.; Chu, W. Novel Brønsted–Lewis acidic di-cationic ionic liquid for efficient conversion carbohydrate to platform compound. *Cellulose* **2020**, *27*, 6897–6908. [CrossRef]
45. Nuntang, S.; Poompradub, S.; Butnark, S.; Yokoi, T.; Tatsumi, T.; Ngamcharussrivichai, C. Novel mesoporous composites based on natural rubber and hexagonal mesoporous silica: Synthesis and characterization. *Mater. Chem. Phys.* **2014**, *143*, 1199–1208. [CrossRef]